Compact Leaky-Wave SIW Antenna with Broadside Radiation and Dual-Band Operation for CubeSats

Compact Leaky-Wave SIW Antenna with Broadside Radiation and Dual-Band Operation for CubeSats

Maksim V. Kuznetcov, *Graduate Student Member, IEEE*, Symon K. Podilchak, *Member, IEEE*, Miguel Poveda-García, Pascual Hilario, Cristian A. Alistarh, *Graduate Student Member, IEEE*, George Goussetis, *Member, IEEE*, José Luis Gómez-Tornero, *Member, IEEE*

***Abstract*—This letter presents a substrate-integrated waveguide (SIW) antenna for CubeSat applications. The compact structure utilizes middle-point feeding and shorting walls to achieve broadside radiation in the far-field at two distinct frequencies. In particular, this dual-frequency behavior is related to the transition from a dominant leaky-wave (LW) on the aperture at lower frequencies to more hybrid radiation (at higher frequencies) due to LW fields and structure resonance due to truncation. This response is generated by the shorting vias at the lateral ends of the SIW antenna. Given these conditions, the developed leaky-wave antenna (LWA) prototype is well matched ($|S_{11}| \leq$ -10 dB) from 23.2 to 23.5 GHz and 24.8 to 25.2 GHz with realized gains of 8 dBi and 6 dBi, respectively. Maximum efficiency (including the connector) is around 87%. Such dual-frequency operation could enable up-link and down-link operation in the K-band. Overall dimensions of the antenna are $2\lambda_0$ x $2.6\lambda_0$ (at the lower frequency). Possible placement on CubeSats can be underneath solar panels, thus increasing the available surface area for solar power harvesting. Also, to the best knowledge of the authors, no similar dual-frequency SIW-LWA has been previously reported.**

I. Introduction

With the rapid development and cost reduction of space launching programs such as Starlink, CubeSat systems have became a relatively low-cost and popular instrument for space researches and Near-Earth communication systems. However, with the decrease in the size of the platform and the frequency congestion in space, the requirement for new implementations and integration of antenna systems for data transmission between earth and satellite is once again a topic of interest. Changing the design of the CubeSat for the specific antenna systems could increase the cost of the launch and can provide additional challenges in platform operation. On the other hand, when considering integration, such changes are necessary for stable communication and efficient operation of the devices on board the satellite.

S. K. Podilchak is with the Institute of Digital Communications, The University of Edinburgh, Edinburgh EH9 3JW, Scotland, United Kingdom. (e-mail: s.podilchak@ed.ac.uk).

Maxim Kuznetcov, George Goussetis, Pascual Hilario and Cristian A. Alistarh are with the Sensors, Signals, and Systems, Heriot-Watt University, Edinburgh EH14 4AS, Scotland, United Kingdom. (e-mail: mk11@hw.ac.uk).

Miguel Poveda-García and José Luis Gómez-Tornero are with the Department of Communication and Information Technologies, Technical University of Cartagena, Cartagena 30202 Spain (email: josel.gomez@upct.es).

Manuscript received March xxxx, 2021. This work was supported by Samsung under the GRO Grant Scheme as well as European Union's Horizon 2020 Research and Innovation Programme under the Marie Skłodowska Curie Project CSA-EU under Grant 709372 and in part by the EU H2020 ITN REVOLVE project under Grant 722840.

Recent antenna designs for CubeSat platform integration have been reflector-type antennas [1], [2]. An example of such an antenna with a CubeSat system was demonstrated in [3]. This antenna primarily consisted of a metallic feeding system and was deployed using a mesh-grid type reflector. The authors investigated different feeding systems to operate at X-band, Ka-band, and X-/Ka-band frequencies while using the same 1-meter size mesh reflector. The antenna demonstrated circular polarization with gains of 36.1 dBic and 48.7 dBic, for X-band and Ka-bands, respectively. The reported antenna efficiency was higher than 62%. The application of such a particular deployable (and perhaps complex) system was for deep-space exploration which is why high gains were required.

Another development for CubeSats are inflatable antennas [4], [5]. Those antennas are based on the material deformation of the surface of the reflector. Such as in [6], the inflatable Kapton type antenna was demonstrated. By heating and deforming Kapton into the parabolic structure and using a feeding system such as a horn antenna, a reflector antenna was made possible. The authors investigated antenna performance considering cylindrical and conical shape deformations of the reflector showing a maximum gain of 15 dBi. In comparison to the mesh-grid type array, the antenna provided a reduced mass, but challenges arose due to the non-ideal parabolic shape of the reflector deformation. As a result, a beam deformation and higher cross-polarization values were observed.

Some other exotic antenna designs were presented in [7] where a linearly-polarized V-band metallic Bull-eye antenna was proposed for communications between a swarm of CubeSats. The antenna consisted of a waveguide feed with multiple grooved rings for radiation and was integrated into the CubeSat chassis body. The reported realized gain was 19.1 dBi at 60 GHz with a directive beam pattern. Additionally, beam-shifting modifications were proposed to steer the beam direction for design flexibility and stable communications between platforms.

Low-profile antennas using standard printed circuit board (PCB) fabrication techniques are also of interest for CubeSat integration due to the possibility of low-cost assembly, compatibility with other planar circuit systems, and also, because they typically need not require any mechanical deployment [8] - [10]. One such antenna presented in [11] used aperture coupled patches for solar cell integration. The antenna provided circular polarization by using radiating and non-radiating patches with a coupler feeding system. The presented antenna operated from about 2.2 GHz to 2.3 GHz with a maximum gain of 6 dBic. The antenna demonstrated an effi-

ciency of 81% and showed that there is no significant impact on the operation of the solar cell. Another antenna system integration was proposed in [12]. In that work [12], a compact linearly-polarized patch antenna operating at 437 MHz was used to communicate between satellites and the Earth station. This work demonstrated successful communication between 5 satellites in the real-test environment (space).

Most of these newly proposed CubeSat antennas for near-Earth applications require a compact and low-cost design that can be easily integrated on the satellite platform. Following these motivations, we propose a compact dual-frequency leaky-wave antenna (LWA) with broadside radiation for K-band applications. Using PCB design techniques, a grounded dielectric slab (GDS) section, and substrate integrated waveguide (SIW) technology [13], the proposed antenna (see Figs. 1 and 2) can reach high efficiencies while maintaining a compact size. Also, the dual-frequency nature of the LWA makes it useful for up-link and down-link satellite communications. It should also be mentioned that some other dual-band LWAs have also been proposed in the literature such as in [14]–[16], however in this letter, the compactness and low-profile of our design can make it suitable for CubeSats.

When considering more conventional planar antenna design techniques in the microwave and the millimeter-wave range, resonant based elements, such as patches and arrays, can suffer from feeding challenges and unwanted surface wave effects reducing radiation efficiencies [17]. Additionally, element coupling in arrays and interference from the satellite structure itself can generate undesired beam patterns as well as increased cross-polarization and side-lobe levels in the far-field. An alternative could be the proposed LWA design with single-point feeding, as such effects might not be as problematic when employing SIW technology, in particular, due to the possible radiation efficiencies and the compact nature of the leaky aperture (which is due to top and bottom metallic patterning and via positioning). These features are also compatible with solar panel placement on top of the SIW-LWA structure itself whilst not covering the compact aperture positioned at the edge of the GDS (see Figs. 1 and 2).

II. General Design Considerations

When considering classic LWA design, to achieve broadside radiation, periodic structures might be required [17], [18]. However, challenges arise to suppress the open-stopband effect which could reduce antenna efficiency [19], [20]. To avoid this, it is possible to design compact LWAs based on the beam splitting condition, which can produce a single beam at broadside due to the combination of a bi-directional leaky-wave (LW) field distribution for radiation on the truncated traveling-wave aperture [18], [21], [22].

Our newly proposed two-sided and truncated design, in this letter, is based on the uni-directional travelling-wave structure previously presented by some of the authors in [23]. For these SIW-LWA structures, the LW phase and attenuation constants, β and α, are controlled by the two parameters W_0 and P_1 within the unit-cell (see Fig. 2 and Table I), which can be tuned in order to work at the splitting condition ($\beta \approx \alpha$) for radiation

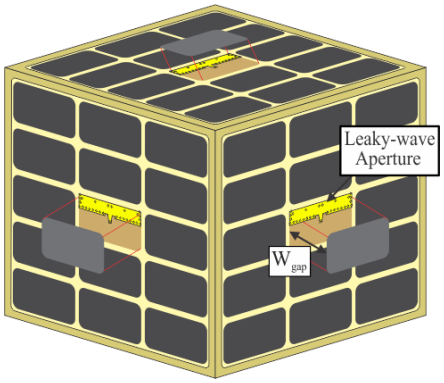

Fig. 1. An example of the proposed LWA integrated on CubeSat and positioned underneath the solar cells, defined by W_{gap}. This simple integration is made possible due to the top and bottom metallic layering by SIW technology. Also, the typical gaps between solar cells (within a solar cell array), can be appropriately spaced for the proposed LW aperture. In this possible implementation, the feed-line (see Fig. 2) could be a replaced by a vertical probe positioned at the center of the SIW.

at broadside and at the desired frequency. Dispersion curves and some preliminary results were presented in [24]. While in this work, structure resonance (by SIW shorting) is further examined for the truncated LWA as well as its dual-frequency response. Full dimensions for the fabricated prototype can be observed in Table I while antenna results are also compared to other planar LWAs found in the literature also proposed for CubeSats (see Table II in the supplementary material).

Based on these design principles, the proposed antenna consists of a bi-directional SIW aperture (see Fig. 2) for LW excitation, hybridized with structure resonance by via wall shorting, defining a truncated structure which can achieve broadside radiation at two distinct frequencies. Structure resonance can be observed in the simulated electric field animations (see the supplementary material) as well as the $|S_{11}|$ plot in Fig. 3 where two distinct minimums in the reflection coefficient are shown. Also, the mid-point feeding generates a 1-D complex LW wavenumber k for propagation along the $\pm x$-directions (as illustrated in Fig. 2, for the first operating frequency and where the E-field is identified in the substrate). This defines a leaky TE-field distribution for the partially open SIW [23]. In general, when LWs are dominant on such an aperture (see Fig. 2(b) in [23]), the E-field is contained within the y-z plane for this type of SIW-LWA.

III. Simulations, Measurements, & Discussions

The proposed LWA was designed using the commercial full-wave simulator CST microwave studio. The manufactured prototype can be seen in Fig. 2. The 90° bend on the feeding 50 Ω microstrip line was introduced to reduce the influence of the connector (end launch 292-04Z-6 from Southwest microwave) on the radiation pattern, which was shown to be slightly degraded when introduced within the full-wave simulator. Also, the tapered transition from the microstrip line to the SIW was optimized to reduce reflections by following [25]. Additionally, the two closely spaced vias that define D_{shadow} (see Fig. 2) were introduced for matching purposes.

The S-parameters measurements were completed using a Keysight PNA N5225A. The antenna is well matched; i.e. with $|S_{11}| \leq$ -10 dB for the frequency ranges of 23 to 23.6 GHz

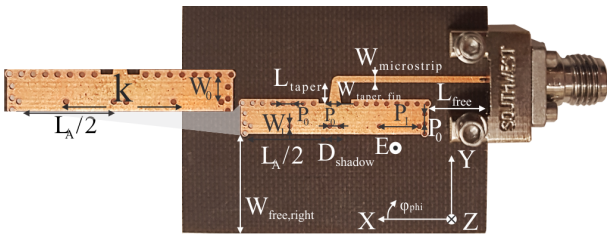

Fig. 2. Fabricated LWA using Rogers RT5880 with a relative dielectric constant of ε_r = 2.33 and thickness h = 0.25 mm with $\tan\delta$ = 0.0009. The antenna dimensions can be found in Table I.

TABLE I
ANTENNA DIMENSIONS (ALL VALUES IN MILLIMETERS, SEE FIG. 2)

$W_{microstrip}$	W_{taper}	L_{taper}	P_0	W_0	W_1
0.79	**1.5**	**3.3**	**1.2**	**2.72**	**0.6**
P_1	D_{shadow}	L_A	L_{free}	W_{free}	W_{gap}
4.66	**1.2**	**20**	**10.9**	**12**	**1**

and 24.8 to 25.3 GHz describing the dual-frequency response (see Fig. 3), with about a 500 MHz of impedance bandwidth for both cases, respectively. At the first frequency (23.3 GHz) radiation is achieved by a dominant LW field on the truncated aperture which is defined by a relatively high normalized LW attenuation constant; i.e. $\alpha/k_0 = 0.27$ (by considering design of the unit-cell and by following [24]), so that the majority of power is radiated; i.e. 90%, adhering to classic LWA design principles [20], as the wave propagates in the SIW from the middle towards the lateral shorting via walls. Now since the structure is truncated, a standing wave effect can be observed in the electric fields (see animations in the supplementary information) due to the remaining LWs (10%) which are not radiated. This achieves resonant behavior for the structure as well as the $|S_{11}|$ minimum.

Considering the second frequency (25 GHz), the normalized leakage rate is reduced (α/k_0 = 0.03) such that some of the unradiated power is further reflected at the lateral shorting walls and travels back towards the feed point. This defines antenna radiation along the truncated aperture to be related to backward and forwarding traveling LW fields for in-phase radiation. An $|S_{11}|$ minimum can also be observed at this second operating frequency; i.e. 25 GHz defining structure resonance. Similar behavior can be observed in [22] where composite right-/left-handed (CRLH) LWAs based on transmission lines experienced multi-band resonance over frequency. For our proposed structure, as in [22], this is also confirmed by the slightly lower efficiency in the second band when compared to the first (see Fig. 4). For example, for the total antenna efficiency it can be seen in Fig. 4 that values reach almost 87% for the first operating frequency and 76% for the second.

In order to evaluate the radiation performance of the pro-

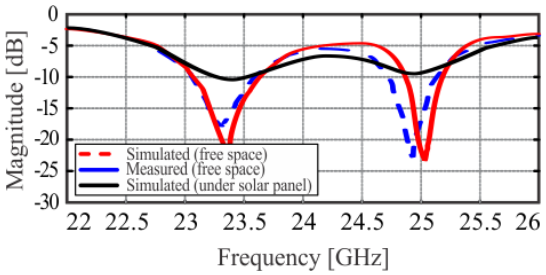

Fig. 3. Simulated and measured $|S_{11}|$ of the proposed SIW-LWA in free-space and with the solar panel on top (simulated), see Fig 1.

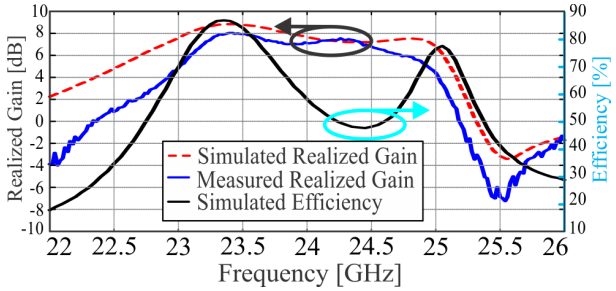

Fig. 4. Measured and simulated realized gain including simulated antenna efficiency. Maximum realized gain can be observed at 23.4 GHz with a value of 8 dBi. The total efficiency including connector losses is also reported where it can be observed that the peak efficiency is 87% at 23.3 GHz.

totype, the NSI-5912 near-field scanner was employed and measurements were completed in the anechoic chamber at Heriot-Watt University. A measured maximum realized gain of 8.0 dBi was observed at 23.4 GHz and 7.2 dBi at about 25 GHz (see Fig. 4). The normalized beam patterns in the ϕ = 90° plane are presented in Fig. 5 and results are in agreement with the simulations. Basically, a directive fan-beam can be observed at 23.1 GHz and beam splitting starts to occur at about 25 GHz (see Fig 5), in that the beam starts to split into two distinct peaks. This suggests frequency beam-scanning like a typical LWA. Measurement results for the ϕ = 0° case are also in agreement with simulations but are not reported due to brevity. Regardless, good broadside radiation is observed but with slightly higher sidelobes at the second frequency. This is related to the bi-directional LW fields on the aperture which do not generate a distinct and single beam maximum (unlike the lower frequency case).

It should also be noted that during antenna simulations, efforts were made to reduce the sidelobes for the higher frequency and maintain a more distinct broadside beam pattern. However, this was not possible without having two beam maximums (at about 25 GHz) being diverted away from broadside (i.e. complete splitting) while also not perturbing the lower frequency pattern.

IV. ANTENNA INTEGRATION ON A CUBESAT PLATFORM

When designing antenna systems it is important to adapt the antenna placement for a particular application. Due to the element size, the antenna can be placed on the side of the CubeSat or underneath a solar cell as illustrated in Fig. 1. However, this single-element can not offer high flexibility in the polarization and the beam pattern. Therefore, we have considered two elements for beam steering and if circular polarization (CP) is of interest, a four-element antenna with quadrature phase excitation. For these cases, the antenna was simulated on the CubeSat with dimensions of 10 cm x 10 cm x 10 cm where the SIW-LWA was placed at the cube center.

In Fig. 6(a) only one element was placed on the center of the CubeSat. In this case, as described above, the SIW-LWA (single-element) offers linear polarization. It should be noted that the maximum realized gain increased to 9.7 dBi (mainly due to the larger effective aperture). There are also slightly higher cross-polarization levels around -60° which are related to the microstrip-type feeding employed in the fabricated design. However, if the feeding system is re-designed considering coaxial or probe-type, cross-polarization values can be improved when satellite placement is of interest.

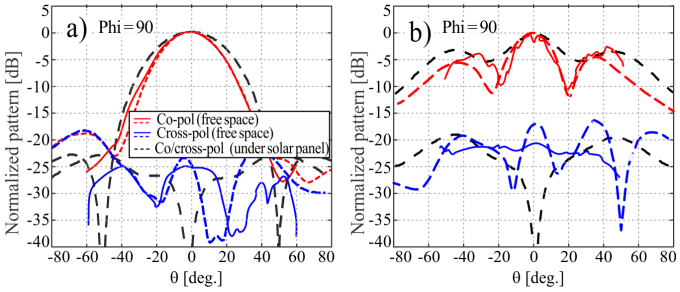

Fig. 5. Simulated and measured (solid line) beam patterns at 23.1 GHz a) and at 24.8 GHz b) in the x-z plane and in the free-space and under solar panel as defined in Fig. 2. Results demonstrate a broadside beam with cross-polarizations well below 15 dB.

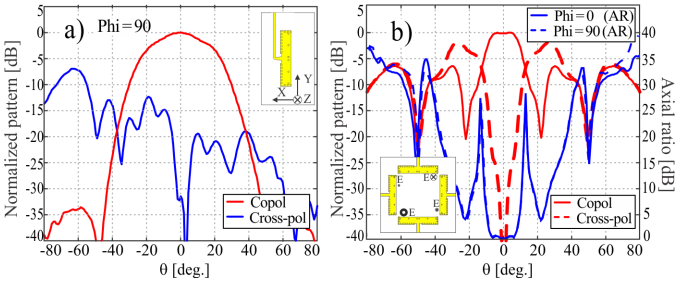

Fig. 6. Simulated antenna configurations on the CubeSat platform with dimensions 10 cm x 10 cm x 10 cm: a) in this case the antenna was simulated as a single element which offered linear polarization. For b) four elements for LHCP; beam pattern (left vertical axis) and axial ratios (ARs), right axis.

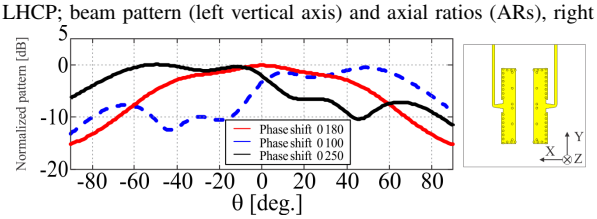

Fig. 7. Simulated two-element pattern considering phase shifts for control of the fan beam pattern in the x-z plane as defined in the inset. In this case, the differential-like feeding offers active matching values below -15 dB.

Four elements for CP were also studied. By applying relative phase shifts of 0°, +90°, +180° and +270° to the elements and defining the 2×2 array arrangement, left-handed circular polarization (LHCP) can be made possible (see Fig. 6(b) and inset). Similar configurations are widely used in CP antenna arrays [26], [27]. Also, a supporting planar circuit feeding system can be integrated onto the CubeSat platform to achieve the noted element phasing. Simulations showed that the system can offer CP which can be useful if reduced polarization losses are important for communications, between the CubeSat and Earth, for example. The maximum simulated realized gain was 9.5 dBic at broadside with cross-polarization levels 40 dB below this maximum. Consequently, axial ratios are well below 3 dB at antenna boresight in both planes (see Fig. 6(b)). However, away from broadside the sidelobe and cross-lobe levels increased since the cross-elements were placed more than 2λ apart defining the generation of grating lobes. Should alternative radiation characteristics be required for the CP case, a varied antenna arrangement would be needed.

In the next study, two elements were placed with the LW apertures separated by about λ/2 and then where excited considering 0° and 180° phase shifts. This array arrangement and feed configuration defines a broadside beam, as in Fig. 7 (red curve), with a maximum gain of 9.6 dBi. The beam steering response can also be observed for this case. This array and differential-feeding reduced the cross-polarization level; i.e. maximum values of -30 dB where observed when compared to the main beam maximum. This steered beam example ($\pm 50°$) could be useful when non-broadside beams are required for communications to other CubeSats, satellites, and in general, when beam steering is needed. Regardless of these findings, using these possible designs the best configuration on the CubeSat platform can be selected which depends on the radiation requirements and space available.

Solar cells can also be placed on the top metal of the SIW structures (see Fig. 1), whilst not covering the LW aperture enabling simple CubeSat integration. To study this scenario further, simulations were also completed when a single SIW-LWA element was placed on the CubeSat and had solar panels on top and around the structure. As reported in [28] [29], [30] typical solar panels consist of a layer of silicon and glass, however, the permittivity, thickness, and conductivity of the silicon can vary significantly. Therefore careful positioning of the solar panels and LWA, with respect to the CubeSat, is required which should be supported by full-wave simulations.

For this study, we used silicon with ε_r = 12 and thickness h = 0.2 mm with a variation of conductivity from 0 to 200 S/m, and, glass with ε_r = 4 having a thickness h = 0.2 mm. As expected, when the solar panels are placed near or on top of the LWA, antenna performance is not significantly affected. However, when positioning on top, it is suggested to have an air gap using a foam type substrate (i.e. ε_r = 1) with a distance which is less than λ/4. Otherwise, the top solar panel starts to act like an unwanted reflector. Considering this, as in Fig. 1, the distance was simulated for various cases and results are reported for when W_{gap} = 1 mm. This placement had a minor mismatch for the proposed LWA which was optimized for free-space conditions. Regardless, as shown in Fig. 3 reflection coefficient values are still below -10 dB at the two operating frequencies. Also, the beam patterns are very similar when considering the free-space scenario (see Fig. 5). Simulations not reported for brevity showed that when the solar cells are positioned more than 1.5 mm, the beam pattern and matching can be disrupted further. Given these findings, if the solar panel integration on top of the antenna is required, the LWA should be co-designed, simulated, and optimized considering the parameters of the selected solar panel whilst avoiding any λ/4 reflections between the solar panel and the LW aperture.

V. Conclusion

A compact SIW-LWA for dual-frequency operation on CubeSats was proposed in this letter. The antenna is well matched from 23.05 to 23.6 GHz and 24.8 to 25.3 GHz with a maximum realized gain of 8 dBi and a peak radiation efficiency of 87%. These features might be useful for up-link and down-link communications in the K-band. Solar cell integration was also considered and other structures were reported using two elements for beam steering or four-elements for CP. Applications include other small satellite commercial missions, earth and planetary observation as well as data links between low earth orbiting satellites. Comparisons to other antennas can be found in Table II (see supplementary information), where it can be observed that no other SIW structures have been investigated for CubeSats whilst offering dual-frequency operation.

REFERENCES

[1] C. Han, J. Huang, and Kai Chang. A high efficiency offset-fed X/Ka-dual-band reflectarray using thin membranes. *IEEE Transactions on Antennas and Propagation*, 53(9):2792–2798, 2005.

[2] N. Chahat, R. E. Hodges, J. Sauder, M. Thomson, E. Peral, and Y. Rahmat-Samii. Cubesat deployable ka-band mesh reflector antenna development for earth science missions. *IEEE Transactions on Antennas and Propagation*, 64(6):2083–2093, 2016.

[3] N. Chahat, J. Sauder, M. Mitchell, N. Beidleman, and G. Freebury. One-meter deployable mesh reflector for deep-space network telecommunication at X -band and ka -band. *IEEE Transactions on Antennas and Propagation*, 68(2):727–735, 2020.

[4] A. Babuscia, B. Corbin, M. Knapp, R. Jensen-Clem, M. Loo, and S. Seager. Inflatable antenna for cubesat: Motivation for development and antenna design. *Acta Astronautica*, 91:322–332, 10 2013.

[5] H. Wang, Fan Bin, Yi Min, F. Guan, L. Guang, C. Xue, Y. Xu, J. Huang, Cai Minghui, and Liu Shihua. Inflatable antenna for space-borne microwave remote sensing. *IEEE Antennas and Propagation Magazine*, 54(5):58–70, 2012.

[6] A. Babuscia, M. Van de Loo, Q. J. Wei, S. Pan, S. Mohan, and S. Seager. Inflatable antenna for cubesat: fabrication, deployment and results of experimental tests. In *2014 IEEE Aerospace Conference*, pages 1–12, 2014.

[7] C. J. Vourch and T. D. Drysdale. V-band "bull's eye" antenna for cubesat applications. *IEEE Antennas and Wireless Propagation Letters*, 13:1092–1095, 2014.

[8] P. Bouça, J. N. Matos, S. R. Cunha, and N. B. Carvalho. Low-profile aperture-coupled patch antenna array for cubesat applications. *IEEE Access*, 8:20473–20479, 2020.

[9] T. Yasin and R. Baktur. Bandwidth enhancement of meshed patch antennas through proximity coupling. *IEEE Antennas and Wireless Propagation Letters*, 16:2501–2504, 2017.

[10] M. J. Veljovic and A. K. Skrivervik. Circularly polarized transmitarray antenna for cubesat intersatellite links in k-band. *IEEE Antennas and Wireless Propagation Letters*, 19(10):1749–1753, 2020.

[11] T. R. Jones, J. P. Grey, and M. Daneshmand. Solar panel integrated circular polarized aperture-coupled patch antenna for cubesat applications. *IEEE Antennas and Wireless Propagation Letters*, 17(10):1895–1899, 2018.

[12] M. Samsuzzaman, M. T. Islam, S. Kibria, and M. Cho. Birds-1 cubesat constellation using compact uhf patch antenna. *IEEE Access*, 6:54282–54294, 2018.

[13] Ke Wu, D. Deslandes, and Y. Cassivi. The substrate integrated circuits - a new concept for high-frequency electronics and optoelectronics. In *6th International Conference on Telecommunications in Modern Satellite, Cable and Broadcasting Service, 2003. TELSIKS 2003.*, volume 1, pages P–III, 2003.

[14] QingLe Zhang, Qingfeng Zhang, Haiwen Liu, and Chi Hou Chan. Dual-band and dual-polarized leaky-wave antenna based on slotted siw. *IEEE Antennas and Wireless Propagation Letters*, 18(3):507–511, 2019.

[15] Yujian Li and Junhong Wang. Dual-band leaky-wave antenna based on dual- mode composite microstrip line for microwave and millimeter-wave applications. *IEEE Transactions on Antennas and Propagation*, 66(4):1660–1668, 2018.

[16] Jan Machá and Milan Polívka. A dual band crlh substrate integrated waveguide leaky wave antenna. In *2011 41st European Microwave Conference*, pages 535–538, 2011.

[17] P. Burghignoli, G. Lovat, and D. R. Jackson. Analysis and optimization of leaky-wave radiation at broadside from a class of 1-d periodic structures. *IEEE Transactions on Antennas and Propagation*, 54(9):2593–2604, 2006.

[18] D. Comite, S.K. Podilchak, P. Baccarelli, P. Burghignoli, and A.P. A. Galli. Analysis and design of a compact leaky-wave antenna for wide-band broadside radiation. *Scientific Reports*, 12 2018.

[19] S. Paulotto, P. Baccarelli, F. Frezza, and D. R. Jackson. A novel technique for open-stopband suppression in 1-d periodic printed leaky-wave antennas. *IEEE Transactions on Antennas and Propagation*, 57(7):1894–1906, 2009.

[20] J. Volakis. *Antenna Engineering Handbook, Fourth Edition*. McGraw-Hill Professional, USA, 2007.

[21] G. Lovat, P. Burghignoli, and D. R. Jackson. Fundamental properties and optimization of broadside radiation from uniform leaky-wave antennas. *IEEE Transactions on Antennas and Propagation*, 54(5):1442–1452, 2006.

[22] Caloz, Christophe and Itoh, Tatsuo and Rennings, Andre. CRLH metamaterial leaky-wave and resonant antennas. *IEEE Antennas and Propagation Magazine*, 50(5):25–39, 2008.

[23] A. J. Martinez-Ros, J. L. Gomez-Tornero, and G. Goussetis. Planar leaky-wave antenna with flexible control of the complex propagation constant. *IEEE Transactions on Antennas and Propagation*, 60(3):1625–1630, 2012.

[24] M. Poveda-García, S. K. Podilchak, G. Goussetis, and J. L. Gómez-Tornero. Millimeter-wave substrate-integrated waveguide based leaky-wave antenna with broadbeam radiation at broadside. In *12th European Conference on Antennas and Propagation (EuCAP 2018)*, pages 1–5, 2018.

[25] F. Taringou, D. Dousset, J. Bornemann, and K. Wu. Substrate-integrated waveguide transitions to planar transmission-line technologies. In *2012 IEEE/MTT-S International Microwave Symposium Digest*, pages 1–3, 2012.

[26] Shih-Kai Lin and Yi-Cheng Lin. A compact sequential-phase feed using uniform transmission lines for circularly polarized sequential-rotation arrays. *IEEE Transactions on Antennas and Propagation*, 59(7):2721–2724, 2011.

[27] Shaowei Liao and Quan Xue. Miniaturized vhf/uhf dual-band circularly polarized four-element sequential-rotation array antenna based on alternately overlapped bent radiation-coupled dual-l antenna elements. *IEEE Transactions on Antennas and Propagation*, 66(9):4924–4929, 2018.

[28] Baoliang Xi, Xianling Liang, Qian Chen, Kun Wang, Junping Geng, and Ronghong Jin. Optical transparent antenna array integrated with solar cell. *IEEE Antennas and Wireless Propagation Letters*, 19(3):457–461, 2020.

[29] Sihao Liu, Deqiang Yang, Yongpin Chen, Xiaokun Zhang, and Yong Xiang. Compatible integration of circularly polarized omnidirectional metasurface antenna with solar cells. *IEEE Transactions on Antennas and Propagation*, 68(5):4155–4160, 2020.

[30] Zheng Zhang, Bowen Bai, Xiaoping Li, Yanming Liu, Chao Sun, and Yanchao Zhang. Integration of circularly polarized microstrip slot array antenna with amorphous silicon solar cells. *IEEE Antennas and Wireless Propagation Letters*, 19(12):2320–2323, 2020.

[31] A. Nascetti, E. Pittella, P. Teofilatto, and S. Pisa. High-gain s-band patch antenna system for earth-observation cubesat satellites. *IEEE Antennas and Wireless Propagation Letters*, 14:434–437, 2015.

[32] S. Li, S. Liao, Y. Yang, W. Che, and Q. Xue. Low-profile circularly-polarized isoflux beam antenna array based on annular aperture elements for cubesat earth coverage applications. *IEEE Transactions on Antennas and Propagation*, pages 1–1, 2021.